UCSF

Title

Mechanisms for focusing mitotic spindle poles by minus end–directed motor proteins

Permalink

https://escholarship.org/uc/item/4z99j1f7

Journal

Journal of Cell Biology, 171(2)

ISSN

0021-9525

Authors

Goshima, Gohta
Nédélec, François
Vale, Ronald D

Publication Date

2005-10-24

DOI

10.1083/jcb.200505107

Peer reviewed

Mechanisms for focusing mitotic spindle poles by minus end–directed motor proteins

Gohta Goshima,[1] François Nédélec,[2] and Ronald D. Vale[1]

[1]The Howard Hughes Medical Institute and the Department of Cellular and Molecular Pharmacology, University of California, San Francisco, San Francisco, CA 94107
[2]The European Molecular Biology Laboratory, Cell Biology and Biophysics Programme, 69117 Heidelberg, Germany

During the formation of the metaphase spindle in animal somatic cells, kinetochore microtubule bundles (K fibers) are often disconnected from centrosomes, because they are released from centrosomes or directly generated from chromosomes. To create the tightly focused, diamond-shaped appearance of the bipolar spindle, K fibers need to be interconnected with centrosomal microtubules (C-MTs) by minus end–directed motor proteins. Here, we have characterized the roles of two minus end–directed motors, dynein and Ncd, in such processes in *Drosophila* S2 cells using RNA interference and high resolution microscopy. Even though these two motors have overlapping functions, we show that Ncd is primarily responsible for focusing K fibers, whereas dynein has a dominant function in transporting K fibers to the centrosomes. We also report a novel localization of Ncd to the growing tips of C-MTs, which we show is mediated by the plus end–tracking protein, EB1. Computer modeling of the K fiber focusing process suggests that the plus end localization of Ncd could facilitate the capture and transport of K fibers along C-MTs. From these results and simulations, we propose a model on how two minus end–directed motors cooperate to ensure spindle pole coalescence during mitosis.

Introduction

In the early stage of mitosis, microtubules become organized into a bipolar spindle, which serves as a dynamic scaffold for aligning chromosomes at the central metaphase plate. In animal somatic cells, centrosomes were thought for many years to be the sole nucleating source of microtubules (herein termed centrosomal microtubules [C-MTs]), which randomly search for and capture kinetochores (for review see Gadde and Heald, 2004; Kirschner and Mitchison, 1986; Wadsworth and Khodjakov, 2004). In meiotic cells or meiotic cell extracts (e.g., from *Xenopus* eggs) that lack centrosomes, microtubules are first nucleated at chromosomes and then become reorganized into bipolar spindles (for review see Compton, 2000; Karsenti and Vernos, 2001)). More recently, it has become appreciated that chromosome-mediated microtubule assembly occurs in somatic cells as well, possibly being nucleated proximal to kinetochores (Goshima and Vale, 2003; Khodjakov et al., 2003; Maiato et al., 2004). Thus, kinetochore microtubules (K fibers [thick bundles of microtubules that connect directly to kinetochores]) originate from both centrosome and chromosome sources. The two path-

ways of microtubule formation have been well documented in *Drosophila* S2 cells (Goshima and Vale, 2003; Maiato et al., 2004), which is the cell type investigated in this study.

Kinetochore microtubules normally become focused toward the two poles, giving rise to the typical diamond shape of the mitotic spindle. However, there is often a visible gap between the minus ends of the focused K fibers and the centrosome, indicating the lack of a direct connection. Moreover, K fibers become focused in the complete absence of centrosomes, as occurs in meiotic cells or in somatic cells that lack functional centrosomes (e.g., after disruption of C-MT nucleation by centrosomin mutations or RNA interference [RNAi] depletion in *Drosophila* [Megraw et al., 2001; and unpublished data]). Thus, the K fibers have an intrinsic focusing mechanism that operates independently of C-MTs. However, the C-MTs also clearly contribute to pole focusing by drawing the K fibers toward the centrosome. This process may result in more tightly focused poles observed in somatic cells as compared with spindles from meiotic cells, *Xenopus* extracts, or centrosomin mutant cells.

The molecules responsible for pole focusing are beginning to become elucidated. In vertebrate cells, a large cross-linking protein called NuMA collects at the minus ends of K fibers, and disruption of this protein leads to splaying of the spindle poles (Merdes et al., 1996). Although different in sequence,

a functionally similar protein called abnormal spindle protein (Asp) appears to mediate an analogous process in *Drosophila* (do Carmo Avides and Glover, 1999; Wakefield et al., 2001). The minus end–directed microtubule motor proteins dynein and the kinesin-14 motors (Ncd in *Drosophila*) also have been widely implicated in spindle pole focusing. Dynein has been shown to transport NuMA to microtubule minus ends (Merdes et al., 2000). However, dynein and Ncd also can cross-bridge microtubules, and the combination of crossbridging and motor activity can collect and focus microtubule minus ends together, as demonstrated in reconstituted assays (Surrey et al., 2001) and in extracts (Heald et al., 1997; Walczak et al., 1998).

Although there is general agreement regarding the participation of minus end–directed microtubule motors in pole focusing, both the respective roles of dynein and Ncd and the mechanistic details by which these motors drive pole focusing remain unclear. Dynein appears to play a dominant role over kinesin-14 in pole-focusing in mitotic spindles in mammalian tissue culture cells (Merdes et al., 2000; Mountain et al., 1999) and in centrosome-containing spindles reconstituted using *Xenopus* meiotic egg extract (Walczak et al., 1997). However, mutations in kinesin-14 members cause severe pole-focusing defects during meiosis and early embryonic mitosis of *Drosophila* (Endow et al., 1994; Matthies et al., 1996), meiosis in mouse oocyte (Mountain et al., 1999), mitosis in Arabidopsis (which lacks cytoplasmic dynein; Ambrose et al., 2005), and in centrosome-free spindles reconstituted using *Xenopus* meiotic extract (Walczak et al., 1998). Even in the same cell type, the literature sometimes has been conflicting on the roles of the two minus end–directed motor proteins. For example, in *Drosophila* S2 cells, Goshima and Vale (2003) reported a large defect in pole focusing with RNAi depletion of Ncd, but not cytoplasmic dynein, whereas Maiato

et al. (2004) reported a substantial pole unfocusing after RNAi knockdown of Dhc64C (Ncd was not examined in this study). More recently, Morales-Mulia and Scholey (2005) reported a qualitative difference in pole unfocusing phenotypes after Ncd and Dhc64C RNAi.

In the present study, our aim was to quantitatively compare the respective roles of Ncd and dynein in pole focusing in *Drosophila* S2 cells and dissect the mechanisms by which these motors contribute to this process. We find evidence for redundancy of Ncd and dynein in pole focusing. However, we also show distinct roles of these motors in different steps of pole focusing (Ncd being required primarily for focusing of the K fibers and dynein being the motor primarily responsible for transporting K fibers along C-MTs toward the centrosome). High-resolution imaging of Ncd-GFP also has provided new information on its mechanism. We find that Ncd is concentrated on the K fibers but exhibits rapid turnover, suggesting that it is not a "static" cross-linker as previously suspected. We also find that Ncd localizes to the microtubule tips of C-MTs, and we propose, based upon computer modeling studies, that microtubule tip–localized Ncd may facilitate minus end–directed transport of K fibers along C-MTs.

Results

Live cell imaging of pole focusing in *Drosophila* S2 cells

To better understand the pole focusing process in *Drosophila* S2 cells, we performed time-lapse imaging of mitotic cells expressing GFP-tubulin. As shown in Fig. 1 A (and Video 1 available at http://www.jcb.org/cgi/content/full/jcb.200505107/DC1), K fibers are generally focused at their minus end. However, this K fiber focusing appears to be a highly dynamic process, as live

Figure 1. **Capture and transport of kinetochore fibers along centrosomal-nucleated microtubules.** (A) A time-lapse image sequence of GFP-tubulin in an untreated (wild-type) S2 cell. Lower panels are enlarged images, and minus ends of K fibers are marked by colored dots. Kinetochore microtubule bundles (K fibers) are cross-linked near their minus ends (e.g., purple dots), followed by focusing to the spindle pole by transport along C-MTs (four dots are gradually focused to the pole during 99–234 s). See also Videos 1 and 2. Bars, 5 and 1 μm. (B) K fiber unfocusing upon C-MTs depolymerization. By replacing culture medium with serum-free medium (SFM), C-MTs are rapidly depolymerized. K fibers gradually shorten and become unfocused. Image acquisition began 30 s after SFM addition. See Fig. S1 for quantitation and see also Video 3 (left). Bar, 5 μm. (C) K fiber focusing upon C-MTs recovery. After 10 min of the serum-free medium (SFM) treatment, large amount of conditioned medium (CM) was added. C-MTs gradually reappeared and accordingly, K fibers became focused. Images acquisition began 60 s after conditioned medium addition (CM). See also Video 3 (right). Bar, 5 μm.
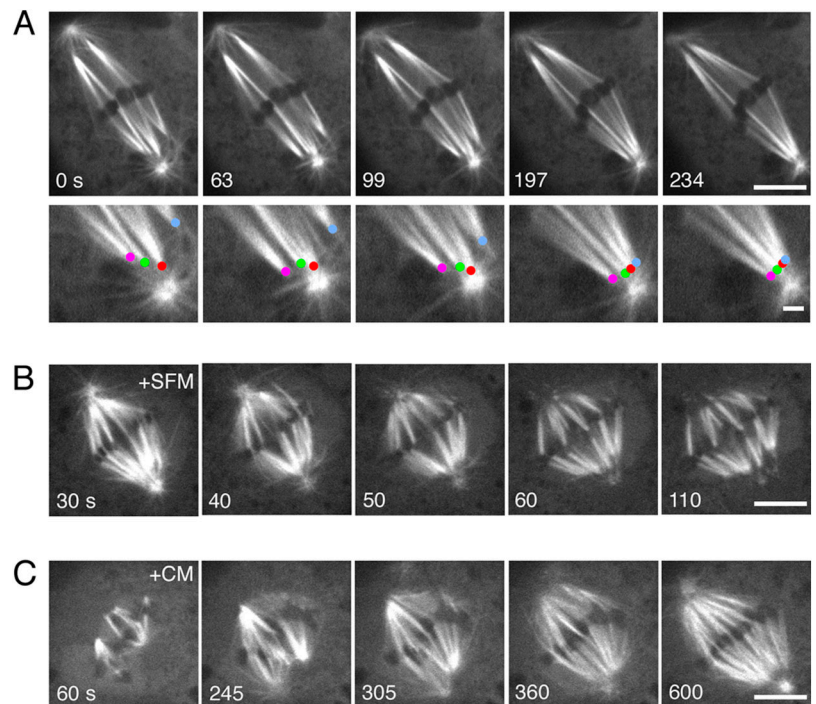
cell imaging shows continuous defocusing/refocusing of K fibers during metaphase (Video 2 available at http://www.jcb.org/cgi/content/full/jcb.200505107/DC1). This dynamic focusing process appears to involve the bundling of K fibers as well as cross-linking of microtubules between K fibers. Such K fiber focusing does not completely depend upon a functional centrosome, as it is observed in cells depleted of centrosomin, albeit often imperfectly (unpublished data). Live cell imaging also shows that K fibers can interact with and transport along C-MTs, resulting in a closer juxtaposition of centrosomes and the minus ends of K fibers and a tighter focus of the pole (Fig. 1 A and Video 1 available at http://www.jcb.org/cgi/content/full/jcb.200505107/DC1). Similar observations also have been reported by Maiato et al. (2004). These findings clearly indicate the separate and sequential processes of initial K fiber focusing and the subsequent transport of the K fibers toward the centrosome.

We also examined the reversibility of pole focusing after a rapid and preferential depolymerization of C-MTs at metaphase followed by repolymerization (Fig. 1, B and C). We found that microtubule depolymerization rapidly takes place in this cell line after replacement of normal cultured medium that contains 10% fetal bovine serum with serum-free medium (see Materials and methods; the molecular mechanism of this phenomenon is under investigation). When serum-free medium was added to metaphase cells, we found that virtually all C-MTs depolymerized very rapidly (<2 min) and the K fibers gradually shortened (Fig. 1 B and Video 3, left, available at http://www.jcb.org/cgi/content/full/jcb.200505107/DC1). Time-lapse imaging and fixed time point staining indicated that upon C-MTs depletion, the K fibers quickly became defocused (74% of cells showed this effect at 4 min; Fig. S1 available at http://www.jcb.org/cgi/content/full/jcb.200505107/DC1). Upon re-addition of serum-containing medium, the C-MTs rapidly recovered and K fiber focusing took place (Fig. 1 C and Video 3, right). Similar K fiber unfocusing was seen upon microtubule depolymerization with colchicine (Video 4 available at http://www.jcb.org/cgi/content/full/jcb.200505107/DC1); however, rapid microtubule recovery was not observed after washing out colchicine. These observations reveal that pole focusing is a dynamic and reversible process that requires integration of C-MTs and K fibers.

Ncd and dynein have selective but overlapping functions in pole focusing

We next performed RNAi of the dynein heavy chain (Dhc64C), Ncd, or double RNAi of both motors and then quantitatively examined pole focusing of metaphase mitotic spindles by fixed cell immunofluorescence (Fig. 2 A). Significant reduction of motor protein levels after a 7-d RNAi treatment was confirmed by immunoblot analysis (Fig. 2 B). We quantitated the two phenomena involved in pole focusing that our live cell imaging suggested as being separable to some extent: the lateral spread of the kinetochore minus ends (herein termed K fiber distance; Fig. 2 C) and the distance between the centrosome and the base of the K fibers (centrosome to K fiber distance; Fig. 2 D). We confirmed the results of Maiato et al. (2004) and Morales-Mulia
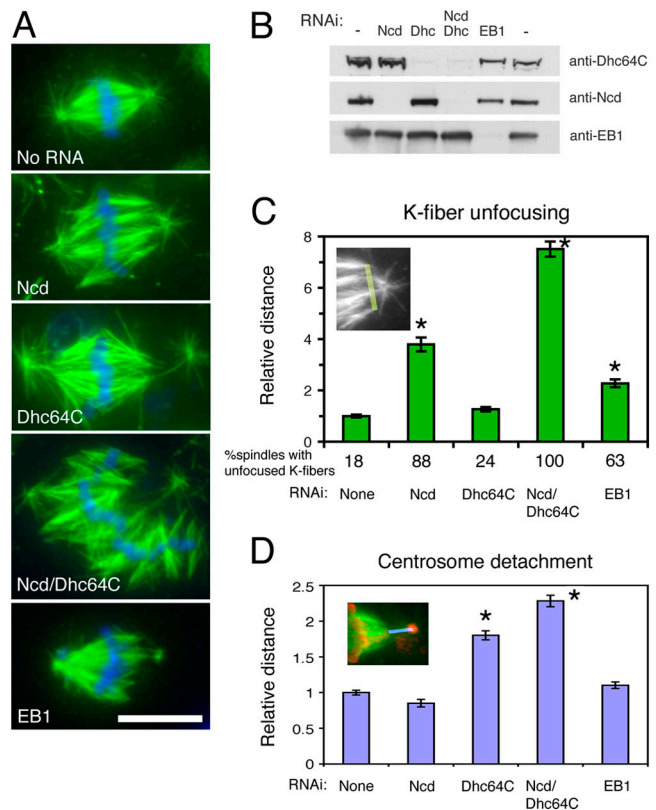

Figure 2. **Distinct effects of Ncd and cytoplasmic dynein on pole coalescence.** (A) Representative spindle morphology after RNAi of indicated genes. Green, tubulin; blue, DNA. Bar, 10 μm. (B) Immunoblot showing knockdowns of indicated proteins. Samples were collected at day 7 after RNAi (dsRNA was treated at day 0 and day 4). Note that single and double RNAi result in similar level of reduction of Ncd or Dhc64C. (C) Quantitation of K fiber unfocusing. Relative mean width of the K fiber minus ends (green line) are shown with standard errors bars (control no RNAi cells; 2.2 ± 1.2 μm [mean $\pm$ SD; $n = 94$]). Experiments were performed twice and combined data is presented. Statistically significant increase was seen after Ncd ($n = 57$), EB1 ($n = 91$) and Ncd/Dhc64C ($n = 59$) double RNAi (asterisk; $P < 0.0001$ for each experiment), whereas Dhc64C single RNAi ($n = 73$) did not produce significant effects at this sample size ($P > 0.05$, t test). The frequency of metaphase spindles with multiple poles or unfocused K fiber(s) was also scored and is described at the bottom ($n > 50$ for each treatment). EB1, Ncd, and double Ncd/Dhc64C RNAi significantly increased the spindles with multiple poles or unfocused K fibers. (D) Quantitation of centrosome detachment in the metaphase spindle. The gap distance between centrosome (stained by γ-tubulin) and the minus end of K fiber that is most closely located to the centrosome was measured in three independent experiments (blue line), and relative average distance to accompanying control sample (average 1.2 ± 0.7 μm [mean $\pm$ SD; $n = 307$]) is shown with standard error bars after single Ncd ($n = 63$), Dhc64C ($n = 188$), EB1 RNAi ($n = 109$), or double Ncd/Dhc64C RNAi ($n = 128$). In each spindle, the pole with the wider gap distance was chosen for measurement. We confirmed that the severe detachment seen after Dhc64C RNAi was not due to prolonged metaphase (Goshima and Vale, 2003), as RNAi of APC/cyclosome component Cdc16 or double Cdc16/Ncd also accumulated in metaphase but such a defect was not observed. Reduction of Ncd often leads to formation of the spindles with multiple asters (Goshima and Vale, 2003). However, we selected the cells whose spindle had overall bipolar structure (i.e., chromosomes are aligned and visible in a single line) and single aster on either side.

and Scholey (2005) of centrosome detachment (an increase in the centrosome to K fiber distance) after Dhc64C RNAi (Fig. 2, A and D). A similar phenotype was observed after RNAi of two dynactin subunits (p50/dynamitin and p150/Glued; unpub-

lished data). Interestingly, Ncd depletion by RNAi did not alter the centrosome to K fiber distance (P > 0.1). However, a weak but statistically significant synergistic effect was apparent upon double RNAi of Ncd and Dhc64C (Fig. 2 D; P < 0.001, compared with Dhc64C alone). In contrast, RNAi of Ncd showed a strong phenotype on K fiber focusing, as was qualitatively described previously (Goshima and Vale, 2003). Maiato et al. (2004) and Morales-Mulia and Scholey (2005) reported that dynein RNAi also caused K fiber unfocusing, but the phenotype was not quantitatively analyzed. We found more K fiber unfocusing in dynein RNAi than control cells, although the effect was much smaller than Ncd RNAi (Fig. 2 C). Again, K fiber unfocusing was much more dramatic after simultaneous knockdowns of Dhc64C and Ncd than each single RNAi (Fig. 2, A and C; P < 0.001). One possible cause of the dramatic synthetic phenotype upon double knockdown could be the presence of polyploidy due to massive failure in previous cell division. However, we did not observe an increase in the DNA content per cell after 7 d Ncd/Dhc64c RNAi treatment (Fig. S2 A available at http://www.jcb.org/cgi/content/full/jcb.200505107/DC1). Moreover, a synthetic pole focusing effect of double RNAi treatment was even observed after a 2-d RNAi treatment, although fewer cells in the population exhibited spindle defects (Fig. S2 B). These results indicate that the synthetic phenotype of double Ncd/Dhc64c RNAi treatment is not due to polyploidy but rather derives from dysfunction of the motors for spindle microtubules.

In summary, these results suggest that Ncd has a major role in K fiber focusing while dynein predominantly prevents centrosome detachment in S2 cells. However, our double RNAi experiments show that these two minus end–directed motors can contribute to both pole focusing activities, which becomes particularly evident when one motor is reduced. In the absence of Ncd, dyneins makes a significant contribution to K fiber focusing, and Ncd also can minimize centrosome detachment when dynein is reduced.

Dynamic localization of Ncd-GFP to the spindle and microtubule plus ends

To better understand the mechanisms of pole focusing, we sought to localize Ncd and dynein/dynactin (a dynein activator) by live cell GFP imaging in S2 cells. We constructed stable cell lines expressing GFP fused to the light intermediate chain of dynein as well as the p50/dynamitin and p150/Glued subunits of dynactin. Even at the lowest levels of expression that were detectable by our microscopy, these constructs displayed diffuse whole cell localization in mitosis as well as some punctate spots that likely correspond to kinetochores (unpublished data). Because we did not observe any clear localization to poles or the spindle that might provide insight into dynein's mechanism in pole focusing, we did not pursue these observations further.

Localization of Ncd was also investigated by stably expressing GFP-tagged Ncd. Functionality of Ncd-GFP for K fiber focusing was confirmed using rescue experiment, in which UTR-based RNAi knockdown of endogenous Ncd was combined with ectopic expression of Ncd-GFP fusion protein (Goshima and Vale, 2005). We also quantitatively measured
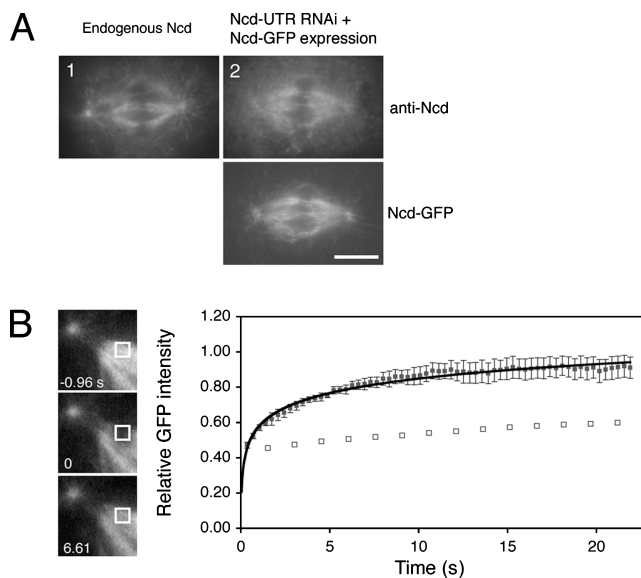

Figure 3. **FRAP studies of K fiber-associated Ncd-GFP.** (A) Comparison of expression levels of Ncd-GFP with endogenous Ncd. A control wild-type cell (1) and a Ncd-GFP–expressing cell in which endogenous Ncd was selectively knocked down by RNAi against UTR region of endogenous Ncd gene (2) were stained with an anti-Ncd antibody. The immunofluorescence intensity of Ncd-GFP in 2 was similar to endogenous Ncd (1). Bar, 5 μm. (B) FRAP experiment reveals dynamic interaction of Ncd with K fiber. (Left) Ncd-GFP fluorescence in the subregion of K fiber (white square) was bleached. (Right) Fluorescence recovery after photobleaching of Ncd-GFP on K fiber. Mean value of relative GFP intensity is shown by square dots with standard deviation (n = 9). Relative GFP intensity was plotted at each time point after normalization using NBA as reference. GFP intensity before bleaching was adjusted to 1.00 (Materials and methods). Immobile fraction was <10% and half time of equilibrium was 2.5 ± 1.0 s, indicating a fast turnover of Ncd-GFP. A FRAP result of GFP-tubulin (subregion of K fiber) is also plotted (open square) and significant fluorescence recovery is not seen in this time range.

the K fiber distance in this rescue condition, and found that Ncd-GFP expression rescued focusing of the fibers to control level (Ncd-GFP expression restored K fiber distance after Ncd RNAi from 5.2 ± 2.3 μm [n = 21] to 2.0 ± 0.6 μm [n = 21], a value close to that of control cells [2.2 ± 1.2 μm]). Unlike dynein, Ncd-GFP was clearly localized to microtubules in the mitotic spindle. To verify that GFP expression levels used for imaging in this study were in a similar range to the endogenous protein level, UTR-based RNAi was performed to deplete endogenous Ncd; Ncd-GFP was then expressed from an inducible promoter and the cells were stained with an anti-Ncd antibody (Fig. 3 A). We then examined low expressing cells that were typically used for live imaging (e.g., Fig. 3 A, 2) and compared the level of anti-Ncd antibody staining with that of endogenous Ncd in control wild-type cells (e.g., Fig. 3 A, 1). The intensity of anti-Ncd staining in the mitotic spindles in the Ncd-GFP–expressing cells was similar to wild-type cells (Fig. 3 A, compare 1 and 2). This level of expression also rescues the Ncd pole unfocusing phenotype (Fig. 3 A, 2). Thus, we believe that imaging of GFP-tagged Ncd in this study was performed under expression conditions that produced comparable levels to the endogenous protein.
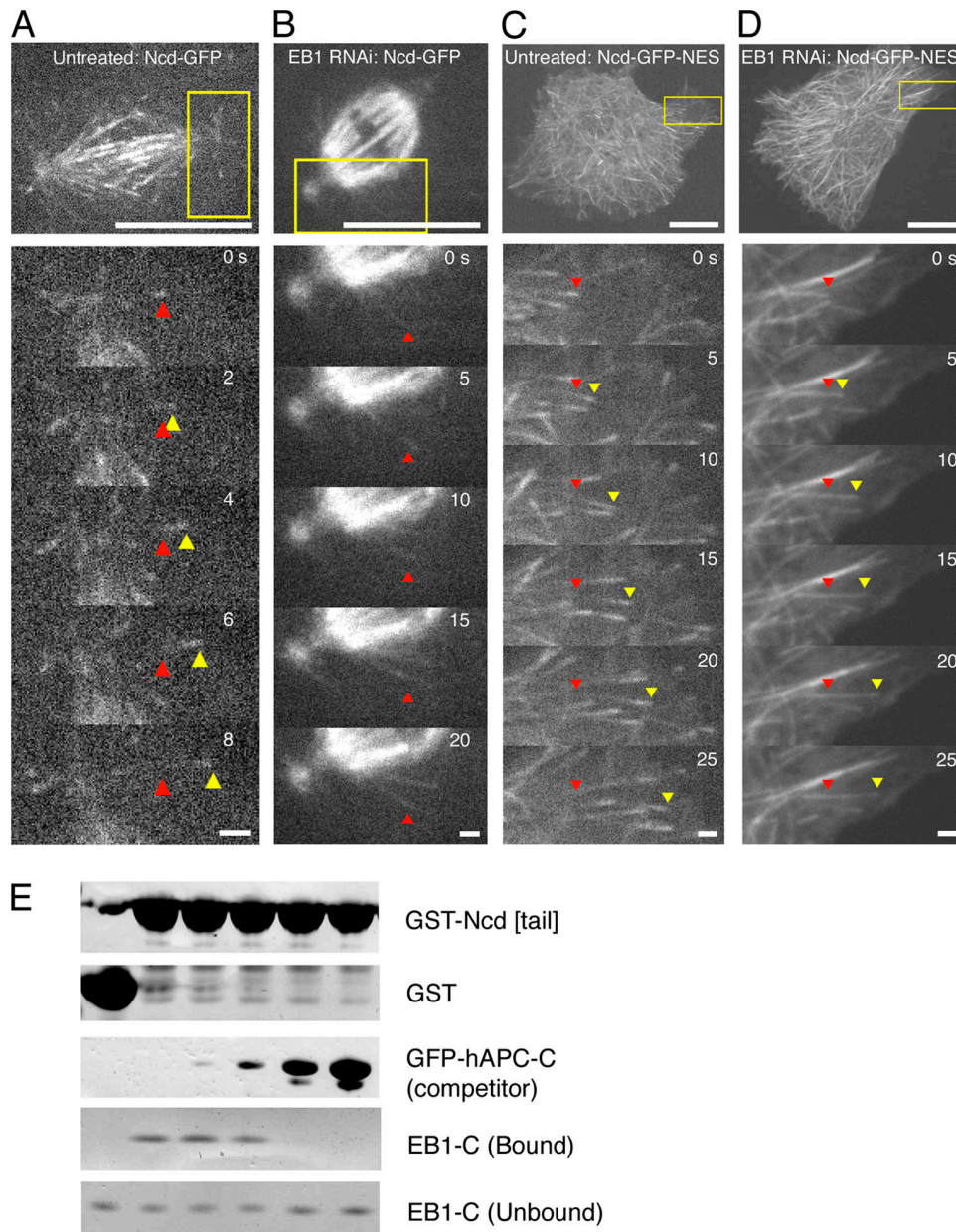
Figure 4. **EB1-dependent, microtubule plus end tracking of Ncd.** (A, top) A still image of Ncd-GFP in the spindle. (Bottom) Time-lapse imaging of the inset region shows tip association of Ncd-GFP on a growing astral microtubule (yellow arrowheads). Red arrowheads indicate the position of the punctate signals detected at time 0. See also Video 5. (B) Ncd-GFP in the spindle in a cell depleted of EB1 by RNAi. Fewer growing microtubules were observed and Ncd-GFP did not accumulate at the tips (arrowheads). See also Video 8. (C, top) A still image of a cell expressing Ncd-GFP-NES. (Bottom) Time-lapse sequences of the inset region. Enrichment of the signals at the growing tip is seen (yellow arrowheads). Red arrowheads indicate the position of the tip signals detected at time 0. See also Video 6. (D) An Ncd-GFP-NES cell after EB1 RNAi (day 7). Accumulation at the tips of growing MTs of Ncd-GFP-NES is not detected (yellow arrowheads). Red arrowheads indicate the position of the tip signals detected at time 0. See also Video 7. Bars of A–D are 10 μm (top images) or 1 μm (bottom images). (E) In vitro interaction of Ncd tail with COOH terminus EB1 fragment. Coomassie staining after GST pull-down experiment is shown. Binding reaction was performed in 200 μl volume with 12 μM dEB1C and 1 μM GST-Ncd-tail (lanes 2–6) or GST (lane 1). GFP-hAPC-C was preincubated with dEB1C at 1:10, 1:3, 1:1, and 2:1 molar ratio for competition (lanes 3–6). Bound fractions were 18-fold loaded compared with unbound fractions.

Live observation of low-expressing Ncd-GFP under wide-field microscope confirmed previous fixed cell immuno-fluorescence and live cell imaging showing enrichment at centrosomes and K fibers (Endow and Komma, 1996). The localization of Ncd to K fibers is consistent with molecular studies on Ncd showing that it can cross-link and bundle microtubules through its COOH-terminal motor domain and a nucleotide-insensitive microtubule binding domain at its NH₂ terminus.

These results suggested that Ncd might serve as a relatively static cross-linking protein that bundles and generates forces upon microtubules (Karabay and Walker, 1999; Wendt et al., 2003). To test this idea of Ncd being a stable cross-linker, we determined the turnover rate of Ncd-GFP on K fibers by FRAP analysis (Fig. 3 B). Surprisingly, the half-time of recovery of a bleached zone in the K fiber was rapid (2.5 ± 1.0 s, $n = 9$). This rate was much faster than recovery of GFP-tubulin in K

fibers (full recovery did not take place during ~30 s observation), which is achieved by spindle poleward flux (microtubule plus end polymerization coupled with minus end depolymerization; Rogers et al., 2005). We also observed that the immobile population of Ncd-GFP was very small (<10%). This result indicates that Ncd-GFP dynamically binds and releases from K fiber and thus is not a static cross-linker in vivo. The dynamic nature of Ncd binding may partly account for the dynamic focusing/defocusing event of K fibers during metaphase.

In addition to the localization of Ncd to K fibers, spinning-disk confocal microscopy revealed a previously unreported enrichment of Ncd-GFP at the tips of growing mitotic microtubules growing from centrosomes (Fig. 4 A, yellow arrowheads; and Video 5 available at http://www.jcb.org/cgi/content/full/jcb.200505107/DC1). Even though the microtubule shafts also have Ncd-GFP staining, our quantitation shows an at least threefold enrichment of the GFP signals at the microtubule tip (unpublished data). The tip localization was most evident in the cells expressing lower amounts of Ncd-GFP (i.e., levels shown in Fig. 3 A, 2; increasing expression led to more uniform staining of the spindle microtubules).

We also tested whether Ncd-GFP localizes to microtubules tips in interphase cells. Normally, Ncd is sequestered in the nucleus during interphase (Goshima and Vale, 2005). However, Ncd-GFP-nuclear export signals (NES) is displaced to the cytoplasm. This construct, at lower levels of expression, also accumulated at the tips of growing microtubules (Fig. 4 C, yellow; Video 6 available at http://www.jcb.org/cgi/content/full/jcb.200505107/DC1). Thus, the plus end–tracking ability of Ncd protein is constitutive and does not appear to be specifically regulated by the cell cycle.

EB1 is a highly conserved microtubule plus end–tracking protein that binds various cargo proteins (e.g., APC [adenomatous polyposis coli protein]; Carvalho et al., 2003; Slep et al., 2005). Ncd also was recently observed to bind to an EB1 affinity column (Rogers et al., 2004). We therefore wanted to investigate whether the plus end accumulation of Ncd-GFP is mediated by EB1. After EB1 depletion by RNAi in Ncd-GFP-NES cell line, we failed to observe a plus end accumulation of Ncd-GFP-NES; instead the microtubules were evenly labeled with this protein (Fig. 4 D; Video 7 available at http://www.jcb.org/cgi/content/full/jcb.200505107/DC1). After EB1 RNAi, microtubules become less dynamic and frequently enter a pause state where they exhibit minimal growth or shrinkage (Rogers et al., 2002). However, even the subset of growing microtubule never accumulated Ncd-GFP-NES at their tips.

We next tested for an in vitro interaction between purified Ncd and EB1 using a GST pull-down assay (Fig. 4 E). We found that the nonmotor "tail" domain (aa 1–290) of Ncd can bind directly to the COOH terminus domain of EB1 (EB1-C; aa 208–278), albeit weakly. This binding was competed by addition of a fragment of human APC protein (2744–2843 aa) that binds to EB1's COOH-terminal domain (Slep et al., 2005), suggesting that the Ncd tail and APC bind to the same site on EB1. However, expression of the Ncd tail domain (1–290 aa) fused to GFP did not track along microtubule plus ends in vivo, suggesting that the motor domain may augment affinity for the microtubules and thereby aid plus end localization (unpublished data).

Similar pole defocusing phenotypes of Ncd and EB1 RNAi

We did not have a specific mutagenesis strategy for eliminating plus end tracking of Ncd while retaining its other critical mitotic activities such as microtubule cross-bridging. However, we examined the consequences of pole focusing and Ncd-GFP localization in mitosis after RNAi of EB1. Time-lapse imaging of mitotic EB1 RNAi cells showed no plus end microtubule enrichment (Fig. 4 B and Video 8 available at http://www.jcb.org/cgi/content/full/jcb.200505107/DC1), as expected from the interphase results described above. However, Ncd-GFP still strongly and dynamically (revealed by FRAP; unpublished data) localized to spindle MTs, indicating that K fiber binding does not require EB1. In this setting of EB1 RNAi where Ncd was mislocalized from microtubule plus ends but not the spindle, we examined centrosome detachment and K fiber focusing. Our previous qualitative study of EB1 RNAi reported both centrosome detachment and pole defocusing (Rogers et al., 2002). When we examined these phenotypes quantitatively here, we found that the EB1 phenotype consists of pronounced K fiber defocusing and has less pronounced centrosome detachment, which is more similar to the Ncd RNAi than the dynein RNAi phenotype (Fig. 2, C and D). Although not definitive proof because EB1 RNAi causes microtubule dynamics defects in addition to displacing Ncd from the microtubule plus end, this result is consistent with a functional link between EB1-dependent localization of Ncd to microtubule tips and K fiber coalescence.

Computer simulations suggest a possible "capture and transport" role for Ncd localized at microtubule plus ends

To explore how minus end–directed motors and EB1 may contribute to the focusing of K fibers at the spindle pole, we applied computer simulations based upon our previous study that simulates establishment of bipolarity of two asters by varying properties of motors (Nedelec, 2002). Specifically, we sought to examine a possible role of an Ncd–EB1 complex at the plus ends of C-MTs. For simplicity, we used a half spindle in a two-dimensional simulation with five K fibers of constant length (6 μm) that have a 10-fold greater stiffness (result of microtubule bundling) compared with single C-MT (Fig. 5 A). The chromosomes to which the K fibers connect at the plus ends were not explicitly represented in the model; instead the fibers were immobilized at their plus end throughout the simulation (Fig. 5 A, white discs). Onto this microtubule array, we added a complex of minus end–directed motors (Nedelec, 2002), which can move toward the minus ends of K fibers and also can cross-bridge a K fiber to a C fiber microtubule thereby exerting forces between the centrosome and the K fiber (Fig. 5 A, green). Although we do not know if such a multiple motor complex exists in the spindle, it could be produced by multifunctional cargos such as Asp or NuMA that could bind multiple motors simultaneously. For our modeling, we endowed this
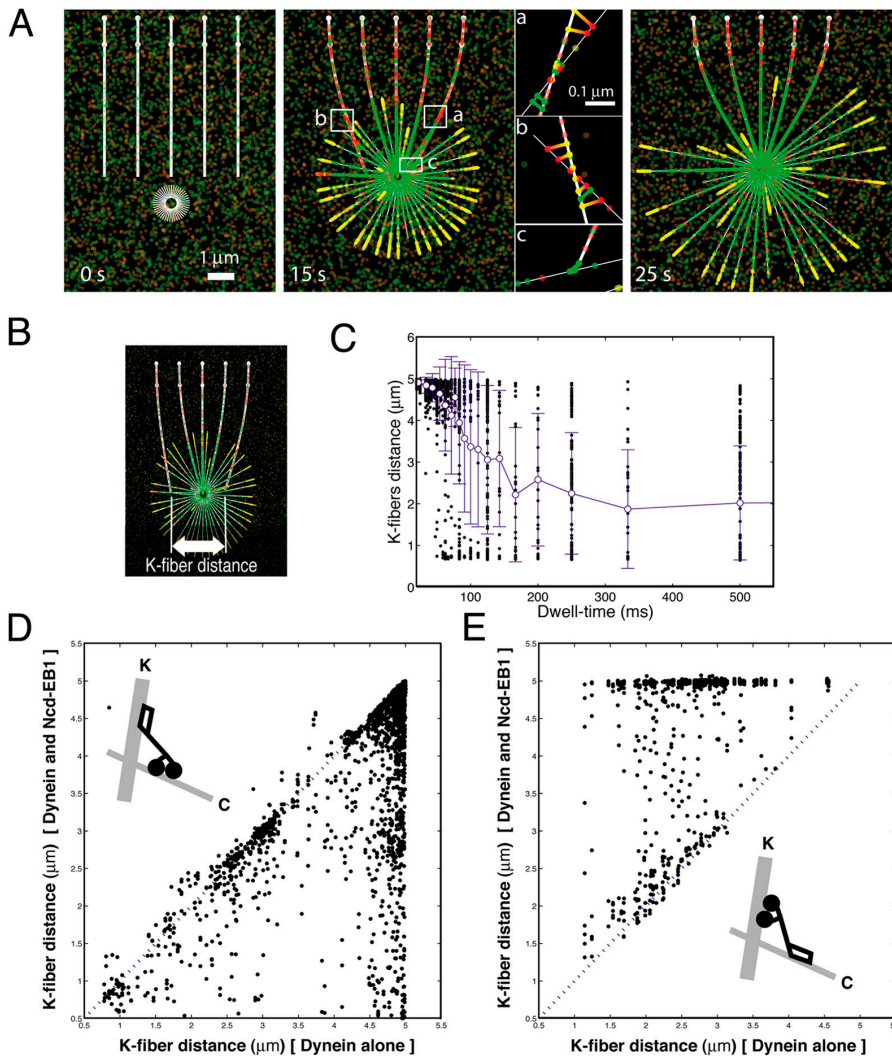
Figure 5. **Computer simulation of pole focusing by minus end–directed motor proteins.** (A) Five K fibers and one aster of dynamic microtubules were simulated to study the pole formation in the mitotic spindle by dynein (green), Ncd (red), and EB1 (yellow) proteins. The K fibers were 10 times stiffer than single astral microtubule, and arranged in a parallel manner with the plus end upward, from which they were held in place firmly, fixed both in position, and rotation (e.g., immobile chromosomes, large white discs). The interaction of K fibers and microtubules was mediated by complexes able to cross-link any two fibers together (see zoomed regions a–c). The time sequence shows the process of K fiber focusing during this simulation. (B) Definition of K fiber distance in the simulation. (C) Influence of dynein dwell-time after reaching the microtubule minus end. Dynein is simulated alone, varying its detachment rate after reaching the minus end, and the other characteristics of the motor (Table I). Because these different parameters are chosen independently, the random sampling can be used to assess the influence of the dwell-time on the focusing. The quality of the focusing is measured likewise experimentally, and varies between 5 μm for nonfocused K fibers to ∼2 μm for a good focusing (see Materials and methods). The points are derived from 2,135 individual simulations and collected in bins based upon different minus end dwell times. The average and standard deviation of the data from these simulations are shown with open symbols (in order to simplify the graph, at dwell-time below 50 ms, circles represent the mean of more than one dwell time). These simulations reveal that the dwell-time has a strong influence on focusing, with a smooth transition around 100 ms. Dynein with a dwell time of 80 ms or more were able to focus the ends very well in some runs. See also Video 9. (D and E) Effect of plus end–localized Ncd–EB1 complexes on K fiber distance (see Table I for each parameter). In the simulations presented in D, the motor domain of Ncd–EB1 complex binds to C-MTs and the nonmotor domain to the K fiber, whereas it is reversed in E (Ncd motor domain binds to K fibers). Each point represents results of K fiber focusing from two simulations: one for dynein alone and one in which dynein was augmented by Ncd–EB1 (various motor parameters used, but the same set of dynein parameter was compared between plus and minus Ncd–EB1). The K fiber focusing result obtained for dynein alone defines the x-axis coordinate, while the focusing obtained after the addition of Ncd–EB1 defines the y-axis coordinate. Points on the diagonal show that Ncd–EB1 did not affect the outcome of dynein-mediated K fiber focusing. Points below the diagonal reveal a positive contribution of Ncd–EB1 to the focusing, while points above reflect a detrimental effect. These simulation reveal that Ncd–EB1, in a configuration where the Ncd motor domain interacts with C-MTs and the nonmotor domain interacts with K fibers, contributes positively to dynein-mediated K fiber focusing (points tend to be below the diagonal), and that this effect is particularly dramatic for simulations in which dynein was less effective for focusing on its own (larger values on the x-axis). In contrast, Ncd–EB1 complex has a strong negative effect on K fiber focusing in the configuration where the motor domain binds to K fibers. See also Video 10.

motor complex with characteristics of dynein (e.g., speeds of 1 μm/s). This is consistent with our RNAi results indicating that dynein is the dominant motor for K fiber transport; however, also note that Ncd may also execute this function, albeit less efficiently, in the absence of dynein (e.g., after dynein RNAi). In some simulations, we also added Ncd–EB1 complex, in which EB1 (Fig. 5 A, yellow) is localized on the ∼1 μm distal plus ends of C-MTs to mimic our finding of microtubule plus end tracking of Ncd (Fig. 5 A, red). Because we do not know whether motor or tail domain of plus end–tracking Ncd binds to K fiber, we investigated the effect of each configuration. To evaluate the outcomes of these simulations, the distance between leftmost and rightmost K fibers was used (Fig. 5 B; analogous to the K fiber focusing measurement in Fig. 2 C).

The simulation is described in more detail in the Materials and methods section. Note that we did not take into account other factors that contribute to pole focusing, such as inter-K fiber cross-linking (driven by Ncd) or other cross-linking factors that may operate at minus ends (e.g., Asp or NuMA).

We first explored the effect of a processive minus end–directed motor complex on K fiber focusing. In general, this motor was endowed with high processivity and fast velocity (characteristic of dynein, which is the predominant motor for K fiber transport along C-MTs), but we systematically varied its various biophysical characteristics (described in Table I; thousands of simulations generated for each case studied; Nedelec, 2002) to explore what parameters are particularly important for K fiber focusing. In these simulations, we found that com-

Table I. **Parameters to use in computer simulation**

Parameter	Value or range of values
General	
Size of the square simulation space	16×16 μm
Overall viscosity of the fluid	$50\times$ water = 50 mPa s
Microtubule rigidity	20 pN μm^2
K fiber rigidity	200 pN μm^2
K fiber length	6 μm
Radius of aster central core (centrosome)	0.2 μm
Number of microtubule in the aster	Random from 13 to 80
Parameters for dynamic instability[a]	
Growth speed	0.16 μm/s
Shrink speed	0.25 μm/s
Catastrophe frequency	0.04/s
Rescue frequency	0.02/s
Dynein	
Number of complexes of two dyneins	250 ~5,000
Binding rate	10 ~50/s
Unbinding rate	0.25 ~2/s
Unbinding rate at the minus-ends	2 ~50/s
Unloaded speed	1 μm/s
Maximum (stall) force	2 ~4 pN
Ncd[b]	
Number of Ncd–EB1 complexes	1,000 ~60,000
Speed	0.16 μm/s
Binding rate	4 ~64/s
Unbinding rate	1.28 to 20.48/s
EB1[c]	
Binding rate	4 ~64/s
Unbinding rate	0.16 ~0.64/s
Length of segment near the plus end where EB1 can bind	0.2 ~0.4 μm

[a]A new microtubule is immediately nucleated after each complete disassembly event.
[b]In our simulation, Ncd can bind anywhere, and detaches immediately the microtubule that would shrink past its binding site (it does not track depolymerizing ends).
[c]EB1 only binds to growing C-MTs (not to K fibers), and detaches immediately when a microtubule shrinks past its position.

plexes of minus end–directed motors can focus K fibers in some cases but not in others. Detailed evaluation of the simulations revealed that more efficient focusing correlates to longer dwell time (i.e., delayed release) of this motor complex after it reaches the minus end of the K fibers (Video 9 available at http://www.jcb.org/cgi/content/full/jcb.200505107/DC1). The effect of dwell time was systematically evaluated in Fig. 5 C. Thus, if minus end–directed motors alone are involved in pole focusing, our analysis suggests that a dwell time of 80 ms or more provides a substantial advantage. It is currently unknown whether purified dynein indeed pauses when it reaches the minus end of a microtubule. It also is possible that other factors may also contribute to this effect. For example, the putative dynein activator NuMA (and possibly *Drosophila* Asp) is enriched at the minus ends of K fibers and such factor could act to effectively delay dynein dissociation at the vicinity of minus

ends. An extremely long delay is unlikely as we do not see dynein accumulation at this region of the spindle by GFP imaging or immunofluorescence. However, effects on pole focusing in this simulation were achieved with a sub-second delay, which would not result in a significant steady-state accumulation.

We next added a plus end–localized Ncd–EB1 complex to our simulations. We first confirmed that Ncd–EB1 alone, regardless of its configuration, could not efficiently focus K fiber minus ends, because this motor has a relatively low speed and processivity (a speed of 0.16 μm/s, with a detachment rate between 1.3 and 20/s; unpublished data). However, from more than 2,000 simulations where dynein is present, we found that the plus end–localized Ncd could aid the K fiber focusing efficiently if the tail domain of Ncd binds to K fibers so that motor domain can engage in minus end–directed transport along the C-MT (Fig. 5 D and Video 10 available at http://www.jcb.org/cgi/content/full/jcb.200505107/DC1). In contrast, and as might be expected, Ncd–EB1 almost always had strong negative effect on focusing in the opposite configuration where the motor domain binds to K fibers (Fig. 5 E). The positive effect of Ncd–EB1 (tail binds to K fiber) is particularly evident in the case where dynein alone cannot focus spindle poles well (e.g., >4.5 μm K fiber distance achieved by dynein alone was sometimes reduced to <1.5 μm by addition of plus end–localized Ncd–EB1; Fig. 5 D). Detailed observation of some individual simulations indicates that the positive effect is derived from two mechanisms (Fig. 5 A, a and b): (1) K fiber transport toward the pole by Ncd, following Ncd attachment to the K fiber with its nonmotor domain and interaction with the C-MT via the motor domains, and (2) cross-linking of K fiber and C-MT by Ncd–EB1 keeps the C-MT plus end in contact with the K fibers, allowing dynein to "zip" the C-MT and K fiber together more efficiently.

In our study, the concentration and parameters of Ncd–EB1 were randomly chosen (Table I), and thus the simulations produced various outcomes in terms of focusing (i.e., decreasing the K fiber distance). To understand which physical parameters are most crucial for improved K fiber focusing, we looked at correlations between parameters of Ncd–EB1 and the extent of focusing. In general, we found that enhancement of the motor activity (e.g., increased number, increased binding rate) acts positively, as expected. However, the most prominent effect was seen for the binding rate of EB1 to the plus ends (unpublished data). This suggests that clustering at the plus ends is critical to allow a low-processivity motor like Ncd to work efficiently as a cross-linker and force generator. Thus, even though these simulations do not include any mechanism by which K fibers may be focused in the absence of a centrosome, they suggest that the Ncd–EB1 complex at the tips of microtubule can act as a facilitator of K fiber focusing.

Discussion

Roles of Ncd and dynein in pole focusing

Based upon our live cell imaging and computer simulation analyses, as well as data from others (Walczak et al., 1998; Maiato et al., 2004), we propose that the coalescence of spindle

poles involves the following steps: (1) inter-K fiber cross-linking, (2) "search and capture" of K fibers by the tip of growing C-MTs, and (3) K fiber transport on C-MTs (Fig. 6). Our RNAi analysis of dynein and Ncd as well as live cell imaging of Ncd-GFP has provided insight into the roles of these minus end–directed motor proteins in these processes. By quantitatively comparing Ncd and dynein knockdown phenotypes in the same cell type, we find that these Ncd and dynein have distinct but overlapping functions in the three steps of pole focusing outlined above.

Our RNAi results suggest that Ncd plays a role in K fiber focusing through three mechanisms described above. Ncd's major role is likely to be in inter-K fiber cross-linking, as evidenced by the splaying of K fibers after Ncd RNAi and the prominent localization of Ncd-GFP to K fibers. This process most likely involves cross-linking of microtubules by Ncd's force generating motor domain and its positively charged "tail" domain that also binds to microtubules independently of the motor. This process occurs in the absence of centrosomes and C-MTs, because acentrosomal spindles created by centrosomin RNAi also show severe K fiber unfocusing when Ncd is also knocked down by RNAi (unpublished observations). We also show that the process of lateral K fiber interactions is highly dynamic, because K fibers are continually splaying and coalescing. Such observations are also consistent with our FRAP measurements of Ncd-GFP, which show that these motors are associating and dissociating with K fibers on a rapid time scale and thus are not behaving as static cross-linkers. Albeit less efficient than dynein, Ncd also likely contributes to minus end–directed transport of K fibers along C-MTs, because the centrosome to K fiber distance is somewhat greater in the Ncd/Dhc64C double RNAi compared with Dhc64C alone. Finally, we believe that Ncd at the tips of C-MTs may act to capture K fibers and facilitate subsequent minus end transport of the K fiber, as will be described in the next section.

Cytoplasmic dynein in S2 cells plays a dominant role in transporting K fibers along microtubules, as evidenced by finding that Dhc64C RNAi causes detachment of centrosomes from the minus ends of K fibers (Fig. 2; Maiato et al., 2004; Morales-Mulia and Scholey, 2005). Although secondary to Ncd, dynein also contributes to the focusing of the minus ends of K fibers. This role of dynein becomes particularly clear after Ncd depletion, as Ncd/Dhc64c double RNAi causes very severe splaying of K fibers. We believe that this K fiber focusing effect also primarily involves dynein's role as a transporter of K fiber bundles along C-MTs, which causes the coalescence of most peripheral K fibers toward the centrosome as shown in our computer simulations. However, dynein may have other roles in K fiber coalescence, such as potentially transporting and concentrating cross-linking proteins (e.g., NuMA and Asp) at minus ends of K fibers (Merdes et al., 2000; Morales-Mulia and Scholey, 2005). Indeed, synthetic effects of kinesin-14 and dynein motors on pole focusing have been reported in centrosome-free spindles reconstituted in *Xenopus* egg extract (Walczak et al., 1998).

The molecular properties of kinesin-14/Ncd and cytoplasmic dynein are well designed to support the above proposed functions of these two motors in pole focusing. Cytoplasmic
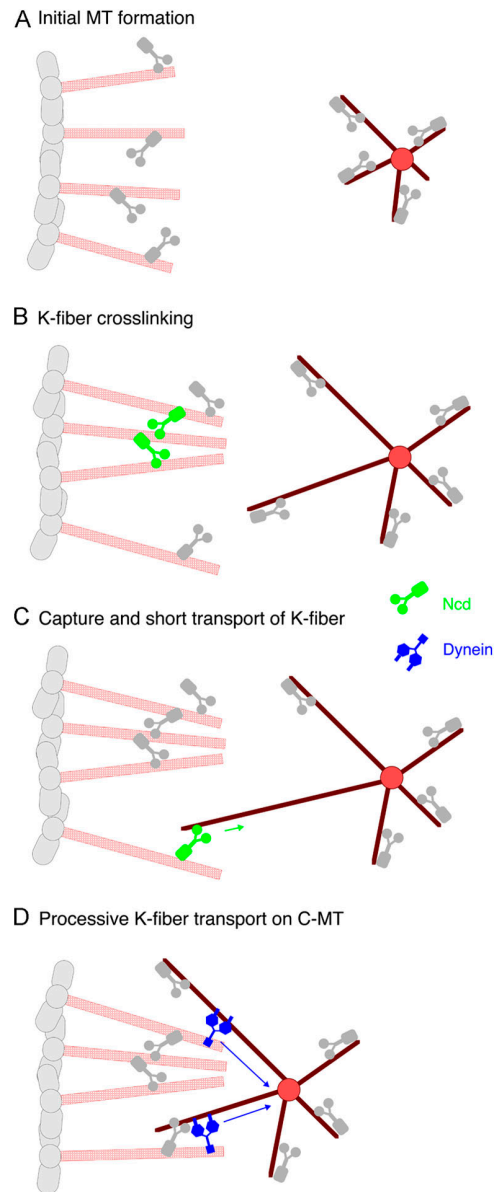

Figure 6. **A model for three-step pole focusing by minus end–directed motors.** (A) During spindle assembly process in early mitosis, or even during metaphase when steady-state length of bipolar spindle is maintained, C-MTs, and kinetochore microtubule bundles (K fibers) are often discontinuous. (B) Inter-K fiber cross-linking by minus end–directed motors (predominantly Ncd in S2 cells). (C) Search and capture of K fibers by Ncd, which is recruited to the microtubule plus end. Note that EB1 protein is required for plus end tracking of Ncd but is not described in this cartoon figure. Because Ncd has two microtubule binding domains, Ncd enables C-MTs to "search" for, then "capture," and generate force upon K fibers. Our computer simulation supports the herein described configuration of Ncd where the nonmotor domain of Ncd binds to K fibers. (D) Next, minus end–directed motors (primarily processive dynein motor) transport the K fibers along C-MTs to the pole (bottom). Our simulations suggest that the search and capture mechanism in C can potentially facilitate such motor-mediated transport. However, in the case where a C-MT locates spontaneously closely to a K fiber, dynein can cross-link and transport the K fiber without the help of plus end–tracking Ncd (top).

dynein is a fast, processive motor (Mallik et al., 2004). Thus, small numbers of dyneins could rapidly transport K fibers along C-MTs. On the other hand, Ncd is nonprocessive, slow

motor that is not designed for cargo transport. Instead, its ability to bind two microtubules and its slow motor activity makes it an effective cross-bridger between microtubules in the spindle. These properties are likely to be advantageous for inter-K fiber cross-linking, as well as for crossbridging of C-MTs plus ends to K fiber. However, the rapid on–off rates of these cross-bridges, as shown by our FRAP data, would still enable dynein to effectively transport the K fibers along the C-MTs.

Our phenotypic RNAi analyses may account for differences in the pole unfocusing phenotypes of Ncd or dynein depletions that have been described in the literature. Specifically, we suggest spindle architecture in the given system (e.g., the presence or absence of centrosome and differences in microtubule dynamics) may determine whether Ncd or dynein acts as the essential contributor to pole coalescence. For example, Ncd/kinesin-14 function, which we show to be particularly important for K fiber focusing, may become more crucial when centrosomes are detached or absent from the spindle. Consistent with this idea, the most dramatic pole unfocusing phenotypes for kinesin-14 mutations/depletions have been described in plant mitosis and animal meiosis, systems in which spindle assembly occurs through a centrosome-independent mechanism and in which interactions between C-MTs and K fibers are simply absent (Yamamoto et al., 1989; Walczak et al., 1998; Ambrose et al., 2005). However, dynein also is likely to play crucial roles in pole coalescence in some acentrosomal spindles, as shown convincingly in *Xenopus* extract system (Walczak et al., 1998). In contrast, somatic animal cell mitosis utilizes centrosomes, and kinesin-14 is less important for pole focusing in such cells (e.g., Ncd is nonessential in fly development; Sharp et al., 2000). Microtubule dynamics, specifically the relative number of K- to C-MTs in the bipolar spindle, also may alter the relative contribution of the two motors. For example, if C-MTs are very abundant, the high probability of close approximation of K- and C-MTs may enable dynein to easily link these two networks without any assistance from kinesin-14 motors at microtubule plus ends (this idea was supported by our computer simulation [unpublished data]).

Ncd tracks plus end of growing microtubules during metaphase

An unexpected finding of this study is the microtubule plus end tracking of Ncd. Localization of a kinesin-14 motor protein to the plus end of interphase microtubules has been recently reported in plants (Ambrose et al., 2005). Ambrose et al. (2005) also shows the accumulation of kinesin-14 at the plus end overlap zone in mitotic spindle but did not resolve whether this localization reflected localization of plus ends of individual microtubules. Nevertheless, their work does suggest that the plus end tracking in mitotic microtubules might be a broadly conserved feature of kinesin-14 motors. Yeast Kar3p also was shown to accumulate at the plus ends of microtubules at the shmoo, but it is more enriched on the depolymerizing microtubules (Maddox et al., 2003), which is not observed for Ncd. Even though we find that C-MTs are still dynamic after Ncd RNAi, it is possible that Ncd at the plus end also modulates microtubule dynamics, as does EB1 or other tip-localized proteins.

The enhanced K fiber unfocusing in EB1 RNAi-treated cells, which displaces Ncd from plus ends but not K fibers, suggests that plus end tracking of Ncd may serve a function in pole focusing. We propose that plus end tracking of Ncd on newly nucleated C-MTs, as a "capture factor," facilitates their connection to K fibers, possibly using its second microtubule binding site located in its NH_2-terminal tail domain (Fig. 6 C). This idea is analogous to the Kirschner and Mitchison "search and capture" model for how C-MTs find chromosomes (Kirschner and Mitchison, 1986). In this case, the tip-localized motor Ncd enables C-MTs to "search" for and then "capture" a second major microtubule network in the spindle, the K fibers (Wadsworth and Khodjakov, 2004). Ncd may generate a connection between K fiber and C-MTs temporary, and thereby facilitate the recruitment of minus end–directed transporter (primarily dynein but Ncd contributing as well) for the transport of K fibers (Fig. 6 D, bottom). Additionally, Ncd at the plus end may act as a K fiber transporter once it binds, although this transport would be less efficient than that produced by fast and processive dynein motors (Fig. 6 C). We also note that our simulations are two-dimensional and encounters between C-MTs and K fibers would become less likely in three dimensions, and one might expect the effect of a C-MT–mediated capture/transport mechanism to become more important under such circumstances.

The microtubule plus end search-and-capture mechanism might apply to other aspects of metazoan cell division. For example, cross-linking interactions between antiparallel microtubules occurs at overlap zone of microtubules, and genetic study demonstrates that Ncd produces an inward force on antiparallel microtubules during early mitosis (Sharp et al., 2000). Ncd at the tips of growing microtubules may act to capture microtubules that arise from the opposite pole. Another possible target of tip-localized Ncd may be free microtubules, which are either released from centrosomes or generated de novo in cytoplasm and are eventually incorporated into the spindle by a dynein-dependent transport process (Rusan et al., 2002; Tulu et al., 2003).

Materials and methods

Cell culture and RNA interference

Drosophila Schneider cell line (S2) was cultured and RNAi was performed according the methods of Clemens et al. (2000). Templates for in vitro transcription were generated by PCR using the primers described in Table S1 (available at http://www.jcb.org/cgi/content/full/jcb.200505107/DC1). The synthesized dsRNA was added to cell culture in 96- or 24-well plates in amounts of 1 or 5 µg, respectively. At the end of the RNAi (days 4–7), cells were resuspended and replated on Con A–coated coverslips typically for 3 h before imaging or fixation (Rogers et al., 2002). RNAi treatment was repeated at day 4 for a 7-d treatment. $CuSO_4$ was added for induction of gene expression (for low level expression, 0–25 µM for >1 d). To induce C-MT depolymerization, we replaced 10% serum-containing medium with serum-free medium for 2–10 min. For cells plated on a glass bottom culture dish (35 mm; Mattek), 1 ml serum-free medium was added. This treatment rapidly and dramatically depolymerizes microtubules, particularly astral microtubules, although the precise mechanism is unknown. For regrowth assay, we replace serum-free medium with conditioned medium that contains 10% serum. Construction of Ncd-GFP cell line is described in Goshima and Vale (2005). Most of the cells (>70%) in this stable cell line express GFP. Note, however, that the expression level of GFP is variable among cells, as we did not perform clonal selection of the cell lines.

Immunofluorescence microscopy

Cells were generally fixed by 6.4% paraformaldehyde for 15 min, followed by 0.5% SDS and 0.1% Triton treatment. Ncd was stained after methanol fixation (Rogers et al., 2002). The following antibodies were used: antitubulin antibody (DM1A; 1:500), anti–γ-tubulin (rabbit: 1:100; T-3559; Sigma-Aldrich), anti-Ncd (rabbit: 1:300). Hoechst 33342 (0.5 μg/ml) was supplied for DNA staining. Specimens were imaged using a cooled CCD camera Sensicam mounted on a Axiovert microscope (Carl Zeiss MicroImaging, Inc.).

Live imaging of GFP-tagged proteins

For time-lapse imaging, images from low-expressing Ncd-GFP cells were collected at 1–2-s intervals with 200–5000-ms exposure times at room temperature (22–25°C) using a cooled CCD camera Orca-ER or ER-II (Hamamatsu) attached to a Yokogawa spinning-disk confocal scanhead (PerkinElmer) that was mounted on either an inverted microscope (TE2000; Nikon) equipped with excitation and emission filter wheels (Sutter Instruments) or a Axiovert microscope (Carl Zeiss MicroImaging, Inc.). Camera and filter wheels (Nikon microscope) or acousto-optic tunable filter (Carl Zeiss MicroImaging, Inc. microscope) were controlled by Metamorph software on a PC computer (Molecular Devices/Universal Imaging Corp.). GFP-tubulin (Goshima and Vale, 2003) was imaged by the same setting with a 20–50-ms exposure time.

FRAP

FRAP was conducted with a microscope (LSM510; Carl Zeiss MicroImaging, Inc.), using a 63×/1.40 NA objective lens and with the pinhole fully opened. The pixel size was 80 nm/pixel. Between 5 and ~100 images were acquired about every 350 ms before and after photobleaching, respectively. The bleached area (BA) was generally fixed at 15×15 pixels. GFP intensity of bleached area was normalized using the intensity of non-bleached K fiber of the same size (nonbleached area; NBA): relative intensity at time t_n was calculated as $BA(t_n)/BA(t_0) \times NBA(t_0)/NBA(t_n)$, where t_0 represents the first time-point of image acquisition (before bleaching).

Biochemistry

For GST-Ncd-tail construction, nonmotor domain of Ncd (1–290 aa) was subcloned into the *Escherichia coli* expression vector pGEX-6P2 by introductions of BamHI and EcoRI sites. This plasmid construct was transformed into BL21 *E. coli* for recombinant expression. Saturated culture grown in Luria-Bertani medium at 37°C was diluted by 1:100 and further incubated for 2 h; temperature was then decreased to 20°C for 30 min, followed by IPTG addition to a final concentration of 0.1 mM. Culture was induced for 16 h and harvested. Bacterial pellet was resuspended in lysis buffer (PBS, pH 8.0, 1 mM DTT, and 1 mM PMSF) and lysed using a microfluidizer (Microfluidics, Inc.). The lysate was clarified by centrifugation at 35,000 *g* for 35 min. Supernatant was incubated with glutathione-Sepharose beads for 1 h at 4°C with rotation. The resin was washed three times with lysis buffer, resuspended with 10% glycerol-containing lysis buffer, and frozen in liquid nitrogen. Control GST protein was purified from pGEX-6P2 plasmid using the same method. Recombinant COOH terminus (208–278 aa) of *Drosophila* EB1 protein (dEB1C; courtesy of Dr. Kevin Slep, University of California, San Francisco, San Francisco, CA) as described for human EB1 (Slep et al., 2005) and GFP-tagged APC COOH terminus construct (2744–2843 aa) was purified by published methods (Slep et al., 2005). For in vitro binding experiments, resins that associate GST or GST-Ncd-tail were washed three times with binding buffer (20 mM Hepes-KOH, pH 7.4, 2 mM EDTA, 1 mM DTT, 150 mM NaCl, protease inhibitor cocktails), and dEB1C protein was added. After incubation for 1.5 h at 4°C with rotation, centrifugation was performed and unbound fraction was collected. Resins were washed twice with binding buffer and SDS-containing binding buffer was added and boiled. For competition experiment, dEB1C was preincubated with GFP-APC-C for 1 h at 4°C.

Computer simulation

We used numerical simulations as previously described (Nedelec, 2002) to explore how microtubule motors and end-binding protein may contribute to the focusing of K fibers in the context of the spindle. For simplicity, and taking advantage of the symmetry, we only simulated five K fibers and a single aster of dynamic microtubules originating from the centrosome (in our simulation, a mechanical solid in which the minus ends of microtubules are embedded; Fig. 5 A). The chromosomes to which the K fibers connect at the plus ends were not explicitly represented in the model; instead each K fibers was immobilized at its plus end throughout the simulation by two fixed unbreakable "clamps" representing harmonic springs of high stiffness (1,000 pN/μm). Kinetochore fibers in *Drosophila* are made of multiple overlapping microtubules, but were simulated here by a single filament of constant length and much stiffer than the individual microtubules emanating from the centrosome (Table I). The K fibers are otherwise identical to the C-MTs, and in particular, motors bind and move on both alike. Because the K fibers are very stiff and were arranged parallel over a width of 5 μm, it is impossible to achieve focusing in the absence of a centrosome. However, this setup can be used to study how diverse combinations of motors and MAPs may contribute to the focusing of the K fibers. The formation of a spindle pole requires moving the aster to the appropriate position from its initial position (Fig. 5 A), and bending the K fibers (against their high rigidity). We explored different combinations of motors by randomizing the unknown parameters in the system (Nedelec, 2002), thus generating thousands of simulations for each case studied. To automatically evaluate the quality of focusing, we defined the K fiber distance as the width that the five K fibers span at their minus ends, averaged over time (from 1,000 to 2,500 s, the initial phase being skipped to reduce the influence of the initial configuration). The best examples of focusing achieved a K fiber distance of ~1 μm, a limitation dictated by the geometry of the setup: the K fibers have the same length of 6 μm, and are attached strongly at their plus ends (Fig. 5 A). By definition of the K fiber distance, a value of 5 μm or more indicates the absence of focusing, while a value of ~3 μm likely indicates that one of the K fibers is unfocused, while the others are focused. All the molecules considered were diffusing complexes able to cross-link at most two microtubules, a microtubule and a K fiber or two K fibers (a very rare event) simultaneously, and without distinction between C-MT and K fibers. EB1 could bind only within 0.2 or 0.4 μm of the plus end of growing microtubules (this excluded K fibers). Because we assumed that bound EB1 would not move, the size of plus end comet would be simply determined by the ratio of microtubule growth rate by the unbinding rate of EB1. Hence, the off-rate of EB1 was randomly chosen to be 0.16, 0.32, or 0.64 (s^{-1}) always ensuring a comet of ~1 μm or less. Ncd was modeled as a minus end–directed motor with a speed 0.16 μm/s, with a randomly chosen unbinding rate between 1.3 and 20.5 (s^{-1}) and could bind anywhere. We explored two hypothesis for how EB1 on a growing C-MT might target Ncd to a K fiber: (1) EB1 stays attached to the C-MT, and the motor domain of Ncd binds to the K fiber, the physical link between EB1 and Ncd remains; (2) EB1 on a C-MT end carries Ncd, which binds to the K fiber by its tail. The interaction between EB1-Ncd is released, Ncd motor domain bind and walks on the C-MT to which EB1 is/was attached, and the remaining physical link is between the motor domain on the C-MT and the tail of Ncd on the K fiber.

Online supplemental materials

Fig. S1 shows K fiber unfocusing upon C-MT depolymerization. Fig. S2 shows quantitation of DNA intensity after Dhc/Ncd double knockdown. Videos 1–3 show dynamic spindle pole focusing visualized by GFP-tubulin, and Videos 4–8 present the microtubule plus end tracking of GFP-tagged Ncd. Videos 9 and 10 present computer simulation data that shows spindle pole focusing by minus end–directed motor proteins. Online supplemental materials are available at http://www.jcb.org/cgi/content/full/jcb.200505107/DC1.

References

Ambrose, J.C., W. Li, A. Marcus, H. Ma, and R. Cyr. 2005. A minus-end directed kinesin with +TIP activity is involved in spindle morphogenesis. *Mol Biol Cell.* 16: 1584–1592.

Carvalho, P., J.S. Tirnauer, and D. Pellman. 2003. Surfing on microtubule ends. *Trends Cell Biol.* 13:229–237.

Clemens, J.C., C.A. Worby, N. Simonson-Leff, M. Muda, T. Maehama, B.A. Hemmings, and J.E. Dixon. 2000. Use of double-stranded RNA interference in *Drosophila* cell lines to dissect signal transduction pathways. *Proc. Natl. Acad. Sci. USA.* 97:6499–6503.

Compton, D.A. 2000. Spindle assembly in animal cells. *Annu. Rev. Biochem.*

69:95–114.

do Carmo Avides, M., and D.M. Glover. 1999. Abnormal spindle protein, Asp, and the integrity of mitotic centrosomal microtubule organizing centers. *Science.* 283:1733–1735.

Endow, S.A., and D.J. Komma. 1996. Centrosome and spindle function of the Drosophila Ncd microtubule motor visualized in live embryos using Ncd-GFP fusion proteins. *J. Cell Sci.* 109:2429–2442.

Endow, S.A., R. Chandra, D.J. Komma, A.H. Yamamoto, and E.D. Salmon. 1994. Mutants of the *Drosophila* ncd microtubule motor protein cause centrosomal and spindle pole defects in mitosis. *J. Cell Sci.* 107:859–867.

Gadde, S., and R. Heald. 2004. Mechanisms and molecules of the mitotic spindle. *Curr. Biol.* 14:R797–R805.

Goshima, G., and R.D. Vale. 2003. The roles of microtubule-based motor proteins in mitosis: comprehensive RNAi analysis in the *Drosophila* S2 cell line. *J. Cell Biol.* 162:1003–1016.

Goshima, G., and R.D. Vale. 2005. Cell cycle-dependent dynamics and regulation of mitotic kinesins in *Drosophila* S2 cells. *Mol Biol Cell.* 16:3896–3907.

Heald, R., R. Tournebize, A. Habermann, E. Karsenti, and A. Hyman. 1997. Spindle assembly in Xenopus egg extracts: respective roles of centrosomes and microtubule self-organization. *J. Cell Biol.* 138:615–628.

Karabay, A., and R.A. Walker. 1999. Identification of microtubule binding sites in the Ncd tail domain. *Biochemistry.* 38:1838–1849.

Karsenti, E., and I. Vernos. 2001. The mitotic spindle: a self-made machine. *Science.* 294:543–547.

Khodjakov, A., L. Copenagle, M.B. Gordon, D.A. Compton, and T.M. Kapoor. 2003. Minus-end capture of preformed kinetochore fibers contributes to spindle morphogenesis. *J. Cell Biol.* 160:671–683.

Kirschner, M., and T. Mitchison. 1986. Beyond self-assembly: from microtubules to morphogenesis. *Cell.* 45:329–342.

Maddox, P.S., J.K. Stemple, L. Satterwhite, E.D. Salmon, and K. Bloom. 2003. The minus end-directed motor Kar3 is required for coupling dynamic microtubule plus ends to the cortical shmoo tip in budding yeast. *Curr. Biol.* 13:1423–1428.

Maiato, H., C.L. Rieder, and A. Khodjakov. 2004. Kinetochore-driven formation of kinetochore fibers contributes to spindle assembly during animal mitosis. *J. Cell Biol.* 167:831–840.

Mallik, R., B.C. Carter, S.A. Lex, S.J. King, and S.P. Gross. 2004. Cytoplasmic dynein functions as a gear in response to load. *Nature.* 427:649–652.

Matthies, H.J., H.B. McDonald, L.S. Goldstein, and W.E. Theurkauf. 1996. Anastral meiotic spindle morphogenesis: role of the non-claret disjunctional kinesin-like protein. *J. Cell Biol.* 134:455–464.

Megraw, T.L., L.R. Kao, and T.C. Kaufman. 2001. Zygotic development without functional mitotic centrosomes. *Curr. Biol.* 11:116–120.

Merdes, A., K. Ramyar, J.D. Vechio, and D.W. Cleveland. 1996. A complex of NuMA and cytoplasmic dynein is essential for mitotic spindle assembly. *Cell.* 87:447–458.

Merdes, A., R. Heald, K. Samejima, W.C. Earnshaw, and D.W. Cleveland. 2000. Formation of spindle poles by dynein/dynactin-dependent transport of NuMA. *J. Cell Biol.* 149:851–862.

Morales-Mulia, S., and J.M. Scholey. 2005. Spindle pole organization in *Drosophila* S2 cells by dynein, abnormal spindle protein (Asp), and KLP10A. *Mol. Biol. Cell.* 16:3176–3186.

Mountain, V., C. Simerly, L. Howard, A. Ando, G. Schatten, and D.A. Compton. 1999. The kinesin-related protein, HSET, opposes the activity of Eg5 and cross-links microtubules in the mammalian mitotic spindle. *J. Cell Biol.* 147:351–366.

Nedelec, F. 2002. Computer simulations reveal motor properties generating stable antiparallel microtubule interactions. *J. Cell Biol.* 158:1005–1015.

Rogers, G.C., S.L. Rogers, and D.J. Sharp. 2005. Spindle microtubules in flux. *J. Cell Sci.* 118:1105–1116.

Rogers, S.L., G.C. Rogers, D.J. Sharp, and R.D. Vale. 2002. *Drosophila* EB1 is important for proper assembly, dynamics, and positioning of the mitotic spindle. *J. Cell Biol.* 158:873–884.

Rogers, S.L., U. Wiedemann, U. Hacker, C. Turck, and R.D. Vale. 2004. *Drosophila* RhoGEF2 associates with microtubule plus ends in an EB1-dependent manner. *Curr. Biol.* 14:1827–1833.

Rusan, N.M., U.S. Tulu, C. Fagerstrom, and P. Wadsworth. 2002. Reorganization of the microtubule array in prophase/prometaphase requires cytoplasmic dynein-dependent microtubule transport. *J. Cell Biol.* 158:997–1003.

Sharp, D.J., H.M. Brown, M. Kwon, G.C. Rogers, G. Holland, and J.M. Scholey. 2000. Functional coordination of three mitotic motors in *Drosophila* embryos. *Mol. Biol. Cell.* 11:241–253.

Slep, K.C., S.L. Rogers, S.L. Elliott, H. Ohkura, P.A. Kolodziej, and R.D. Vale. 2005. Structural determinants for EB1-mediated recruitment of APC and spectraplakins to the microtubule plus end. *J. Cell Biol.* 168:587–598.

Surrey, T., F. Nedelec, S. Leibler, and E. Karsenti. 2001. Physical properties determining self-organization of motors and microtubules. *Science.* 292:1167–1171.

Tulu, U.S., N.M. Rusan, and P. Wadsworth. 2003. Peripheral, non-centrosome-associated microtubules contribute to spindle formation in centrosome-containing cells. *Curr. Biol.* 13:1894–1899.

Wadsworth, P., and A. Khodjakov. 2004. E pluribus unum: towards a universal mechanism for spindle assembly. *Trends Cell Biol.* 14:413–419.

Wakefield, J.G., S. Bonaccorsi, and M. Gatti. 2001. The *Drosophila* protein asp is involved in microtubule organization during spindle formation and cytokinesis. *J. Cell Biol.* 153:637–648.

Walczak, C.E., S. Verma, and T.J. Mitchison. 1997. XCTK2: a kinesin-related protein that promotes mitotic spindle assembly in *Xenopus laevis* egg extracts. *J. Cell Biol.* 136:859–870.

Walczak, C.E., I. Vernos, T.J. Mitchison, E. Karsenti, and R. Heald. 1998. A model for the proposed roles of different microtubule-based motor proteins in establishing spindle bipolarity. *Curr. Biol.* 8:903–913.

Wendt, T., A. Karabay, A. Krebs, H. Gross, R. Walker, and A. Hoenger. 2003. A structural analysis of the interaction between ncd tail and tubulin protofilaments. *J. Mol. Biol.* 333:541–552.

Yamamoto, A.H., D.J. Komma, C.D. Shaffer, V. Pirrotta, and S.A. Endow. 1989. The claret locus in *Drosophila* encodes products required for eye-color and for meiotic chromosome segregation. *EMBO J.* 8:3543–3552.